Journal of Modern Physics, 2018, 9, 753-774
http://www.scirp.org/journal/jmp
ISSN Online: 2153-120X
ISSN Print: 2153-1196

Vibrational and Electronic Spectra of 2-Phenyl-2-Imidazoline: A Combined Experimental and Theoretical Study

Yeddu Sushma Priya[1], Kokkiripati Ramachandra Rao[2], Pallavajhula Venkata Chalapathi[3], Adamilli Veeraiah[4*]

[1]Department of Physics, Adikavi Nannaya University, Rajamahendravaram, India
[2]Crystal growth and Nano Science Research Centre, Department of Physics, Government College (A), Rajamahendravaram, India
[3]Department of Physics, University College of Engineering, Javaharlal Nehru Technological University, Guntur, India
[4]Molecular Spectroscopy Laboratory, Department of Physics, DNR College (A), Bhimavaram, India
Email: *avru@rediffmail.com

How to cite this paper: Priya, Y.S., Rao, K.R., Chalapathi, P.V. and Veeraiah, A. (2018) Vibrational and Electronic Spectra of 2-Phenyl-2-Imidazoline: A Combined Experimental and Theoretical Study. *Journal of Modern Physics*, **9**, 753-774.
https://doi.org/10.4236/jmp.2018.94049

Received: January 20, 2018
Accepted: March 27, 2018
Published: March 30, 2018

Abstract

The structural properties and vibrational frequencies of 2-phenyl-2-imidazoline have been investigated using theoretical and techniques by which a good correlation was observed. The assignments of the vibrational modes were performed with the help of normal co-ordinate analysis following the Scaled Quantum Mechanical Force Field methodology. Natural bond orbital analysis and the highest occupied molecular orbital-lowest unoccupied molecular orbital gap analysis have been carried out. UV-visible spectrum of the compound was recorded and compared with the theoretical UV-visible spectrum of the title molecule using Symmetry Adapted Cluster-Configuration Interaction method which yielded good agreement. Our results reflect that the title compound can be used as good source of UV light.

Keywords

2-Phenyl-2-Imidazoline, DFT, FT-IR, FT-RAMAN, NBO, HOMO and LUMO

1. Introduction

At present, there is an enormous deal of scientific attention in the field of Imidazoline derivatives. Imidazoline is a nitrogen compound and it can be utilized in organic dyes as nitrogenous electron donors since it introduces additional electron donors at position 2. Because of high molar extinction coefficient, Imidazoline and other molecular structures containing nitrogen developed as metal

free organic dyes. Usually, metal-free organic dyes have the apparent molecular structure of the electron donor element and the acceptor element connected by the conjugated chain (D–π–A). 2-imidazoline is a one of the isomers derived from the imidazole. Imidazoline derivatives are pharmaceutically and biologically very significant. Imidazolines exhibit major pharmacological and biological activities such as antidepressive [1], antihyperglycemic [2], antihypercholesterolemic [3], anti-inflammatory [4] and antihypertensive [5]. The drug clonidine containing Imidazoline is used independently otherwise it is used with the combination of other medications for the therapy of high blood pressure. Imidazoline and its derivatives are important sort of inhibitors which could effectively inhibit corrosion of carbon steel against CO_2 and H_2S [6] [7]. Recently C.D. Contreras *et al.* [8] reported the structural and vibrational analyses of 2-(2-benzofuranyl)-2-imidazoline.

The purpose of this study is to obtain the theoretical information about the molecular structure and electronic parameters of 2-phenyl-2-imidazoline. Density functional theory has been adopted for the precise study of the molecular geometry and electronic distribution. Here we study the experimental and theoretical study of the 2-phenyl-2-imidazoline for the first time.

2. Experimental Studies

The powder sample of 2-phenyl-2-imidazoline (here after termed as 2PI) has been procured from sigma Aldrich chemical company (USA) with a confirmed purity greater than 98% and was utilized in the consequent spectroscopic study with no any additional purification.

2.1. FT-IR Spectrum

Fourier transform infrared spectrum of the 2PI is recorded at the temperature 302.15˚K in the region 4000 - 400 cm^{-1} by Nicolet 6700 FTIR spectrometer fitted by means of a Thermo Nicolet Continuum IR microscope and through a Renishaw in via., Raman microscope with UV or visible laser excitation at a resolution of ±1 cm^{-1}. FTIR spectrum of the given compound was recorded by KBr pellet method with Spectrum GX Fourier transform-infrared spectroscopy (FT-IR) spectrometer.

2.2. FT-Raman Spectrum

The FT-Raman spectrum of the molecule was recorded at a 4 cm^{-1} resolution through a Nicolet Magna 750 Raman spectrometer functioned with an InGaAs (Indium Gallium Arsenide) semiconductor detector in the 3500-0 cm^{-1} region. The excitation source utilized was the 1064-nm line from Neodymium: Yttrium Aluminum Garnet laser. The laser power at the sample location was typically 500 mW.

2.3. UV-Vis Spectrum

UV-Vis spectrum of the 2PI has been recorded in the region of 200 - 400 nm with a Perkin Elmer Lambda 35 UV-vis spectrometer. All the data were recorded

after 1 cycle, with a period of 1 nm, slit width of 2 nm and scan rate of 240 nm·min^{-1} by the spectral resolution of 0.05 - 4.0 nm. The slit width was situating to 15 nm for the emission monochromator and to 10 nm for the excitation monochromator.

3. Computational Details

Quantum chemical density functional computations on 2PI were carried out using Becke's three-parameter (B3LYP) hybrid DFT level employed to optimize the molecular geometry through the 6-31G(d, p) basis set using Gaussian 09W Revision-A.02 SMP [9], Gauss view 5.0.8 molecular visualization program package [10]. The vibrational frequencies are computed through the second order derivative of the energy with 6-311++G** basis set. In this study, it is noticed that the theoretically computed frequencies were slightly more than the experimentally observed frequencies. For a better match between the calculated and experimental frequencies, scaling is carried out on the calculated frequencies. Scaling was executed in accordance with scaled Quantum mechanical (SQM) process [11] [12] [13]. The depictions of the calculated frequencies all over the scaling process were followed by means of the potential energy distribution (PED) matrix. The classification of the normal modes through potential energy distribution (PED) was performed through the MOLVIB −7.0 Program written by Prof. T. Sundius [14] [15]. Natural bond orbital (hereafter, it is abbreviated as NBO) calculations [16] were performed to recognize the hyper conjugation or intra-molecular delocalization with the implementation of NBO 3.1 program in the Gaussian 09W Revision-A.02 SMP version [9] package at the DFT/B3LYP level.

3.1. The Prediction of Raman Intensities

The Raman activity (Si) computed by Gaussian 09W Revision-A.02 SMP version [9] and altered through scaling process with MOLVIB were modified to relative Raman intensity (I_i) by the subsequent equation as of the basic theory of Raman scattering [17] [18].

$$I_i = \frac{f\left(\nu_0 - \nu_i\right)^4 Si}{\nu_i\left(1 - \exp\left(\frac{-hc\nu_i}{kT}\right)\right)} \tag{1}$$

Here ν_i is the normal mode vibrational wave number; ν_0 is the exciting frequency (in cm^{-1} units); h, c and k are the universal constants and f is appropriately chosen common normalization factor used for all the intensities. Pure Lorentzian band shapes were employed to draw simulated FTIR and FT-Raman spectra.

4. Results and Discussion

4.1. Molecular Geometry

The title compound 2PI has a non-planar structure with C_1 symmetry, 21 atoms

and therefore it has 57 normal modes of internal vibrations. The vibrational harmonic frequencies of the given molecule are computed with Density Functional Theory with Becke-3-Lee–Yang–Parr (B3LYP) method [19]. The optimized structure parameters of 2PI computed by DFT/B3LYP level by means of 6-31G(d, p) basis set are represented in **Table 1** in accordance with the atom numbering given in **Figure 1**. The potential energy surface (PES) scan for C3-C4-C5-H15 was detected by varying the torsion angle for each 10˚ up to 360˚ rotation around the bond using 6-31G(d, p) basis set. The graph between the potential energy and the dihedral angle was represented in **Figure 2**. The minimum energy acquired from potential energy surface scan was 454.9756695 Hartrees.

The theoretically calculated optimized geometrical parameters were compared with the single crystal XRD data of 2-[2-(2-Hydroxyethoxy) phenyl]-4, 4, 5, 5-tetramethyl-2-imidazoline-1-oxyl 3-oxide [20] data since the crystal data of the title molecule is not available. It was studied that here a few differences in the investigational and calculated geometrical parameters. These differences might

Table 1. Optimized geometrical parameters of 2-phenyl-2-imidazoline obtained by B3LYP/ 6–311+G** density functional calculations.

Bond length(A^0)[a]			Bond angle(°)[a]		
B3LYP/6-31G(d,p)		Exp	B3LYP/6-31G(d,p)		Exp
C1-N11	1.445	1.498[b]	N11-C1-C2	101.2	101.3[b]
C1-C2	1.528	1.550[b]	C1-C2-N10	106.2	102.1[b]
C2-N10	1.488	1.488[b]	C1-C2-H14	113.3	-
C3-N10	1.311	1.341[b]	N10-C3-N11	115.9	108.8[b]
C3-N11	1.377	1.346[b]	C3-C4-C5	119.5	120.7[b]
C3-C4	1.485	1.458[b]	C3-C4-C7	120.7	119.9[b]
C4-C5	1.399	1. 381[b]	C5-C4-C7	119.6	119.4[b]
C4-C7	1.399	1.391 [b]	C2-C1-H20	112.5	-
C7-H18	1.085	0.930[b]	C9-C8-C6	120.0	121.5[b]
C7-C9	1.397	1.352[b]	C8-C6-C5	120.0	119.3[b]
C9-C8	1.394	1.394[b]	C6-C5-C4	120.1	119.3[b]
C8-C6	1.394	1.369[b]	C4-C7-H18	119.6	119.4[b]
C6-C5	1.396	1.394[b]	C9-C7-H18	119.6	119.4[b]
C9-H19	1.087	0.930[b]	C7-C9-H19	119.9	120.4[b]
C8-H17	1.086	0.930[b]	C8-C9-H19	119.9	120.4 [b]
C6-H16	1.086	0.930[b]	C9-C8-H17	120.0	119.2[b]
C5-H15	1.087	0.930[b]	C6-C8-H17	119.9	119.2[b]
			C8-C6-H16	120.1	120.4[b]
			C5-C6-H16	119.8	120.4[b]
			N11-C3-C4	122.5	125.6[b]
			N10-C3-C4	121.5	125.5[b]

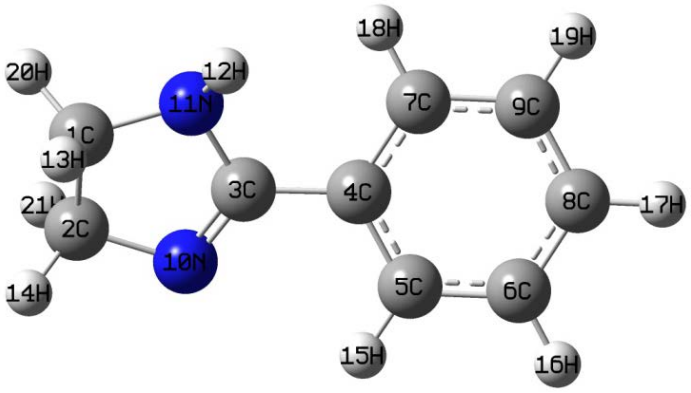

Figure 1. Molecular structure of 2-phenyl-2-imidazoline along with numbering of atom.

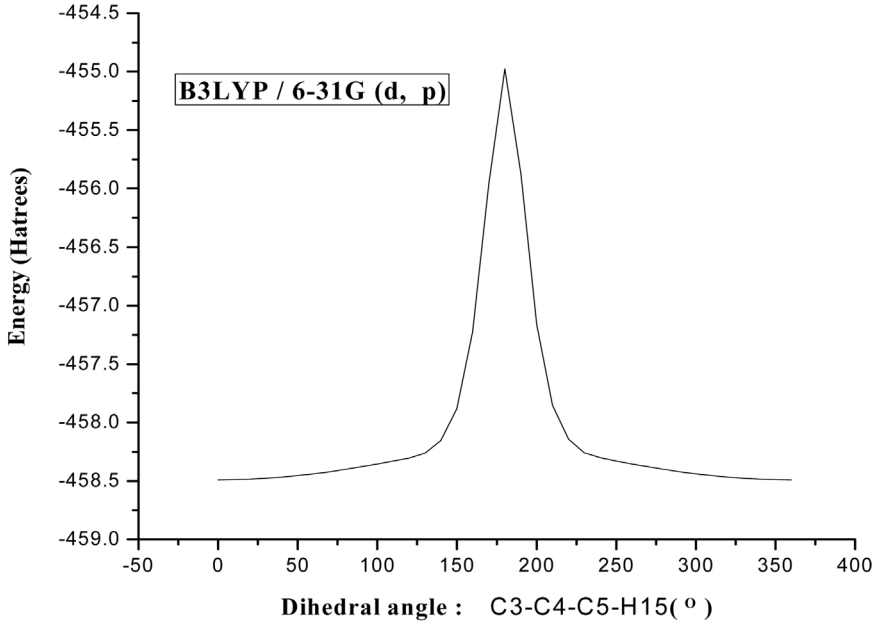

Figure 2. Potential energy surface scan for dihedral angle C3-C4-C5-H15 of 2-phenyl-2-imidazoline.

be because of the intermolecular interactions during the crystalline state. Further, it is noticed that the differences are more for C-H bonds and less for the C-C and C-N bonds. The differences are of the order of 0 A˚ ± 0.156 A˚ for the Bond length when compared with the investigational data [20]. It is observed that the theoretical values are somewhat more than the experimental values for bond lengths. This difference may be because of the cause that the theoretical computations were meant by the molecule in the gaseous phase isolated compound and the experimental outcomes were meant by the molecule in the solid phase. Additionally it is observed that the bond angles are in reasonable agreement with the experimental data of the corresponding observed theoretical data. In spite of the above differences the calculated geometries are used as a foundation to calculate the properties of the molecule such as vibrational frequencies,

polarizability and other properties which are discussed in the following sessions.

Both infrared and Raman spectra. A complete description of fundamental vibrational frequencies of the title molecule was given by Normal coordinate analysis. For this purpose a set of internal coordinates are defined in **Supplementary Material 1**. The local and non redundant symmetry coordinates are defined from these predefined internal coordinates following the recommendations of Fogarasi and Pulay [21] [22]. The detailed description of symmetry coordinates and their respective scale factors are reported in **Table 2**. The simulated and experimental FTIR and FT Raman spectra are shown in **Figure 3** and **Figure 4** respectively.

The title molecule belongs to C_1 symmetry. The 57 modes of vibrations of the molecule are distributed as 39 in plane and 18 out of plane modes. All the vibrational modes are active in:

4.2. Vibrational Analysis

4.2.1. C-H Vibrations

Aromatic compounds have one or more sharp peaks of weak or medium intensity between 3100 - 3000 cm^{-1} [23]. The expected five C-H stretching vibrations of the title compound correspond to mode nos. 13 - 17 of the benzene ring. A weak band observed at 3065 cm^{-1} FT-Raman spectrum belongs to the cluster consisting of the five C-H stretching vibrational bands. The vibrations are shown in PED matrix with percentage about 99%.

The C-H in-plane bending vibrations of benzene and its derivatives are observed in the region 1300 - 1000 cm^{-1} [24]. In this region the bands are sharp, but are of weak to medium intensity. The calculated frequency 1122 cm^{-1} is assigned to C-H in-plane bending vibration and this is in good agreement with the recorded FT-IR spectrum at 1122 cm^{-1}. The C-H out of plane bending vibrations are observed at frequencies at 986 cm^{-1} and 915 cm^{-1} which are coinciding very well with the experimental FT-IR Spectrum at 983 cm^{-1} and FT-Raman Spectrum at 912 cm^{-1} respectively. The Maximum PED distribution is 68% for C-H out of plane bending vibrations. The Remaining calculated C-H out of plane bending vibrations is observed at frequencies 955 cm^{-1}, 840 cm^{-1} and 720 cm^{-1} with a PED Distribution of 41%, 39%, and 55% respectively.

4.2.2. Methylene Group Vibrations

The asymmetric CH_2 stretching vibration is generally observed in the region 3000 - 2900 cm^{-1}, while the CH_2 symmetric stretch will appear between 2900 and 2800 cm^{-1} [25] [26] [27]. The CH_2 asymmetric stretching vibrations are assigned to calculated frequencies at 2955 and 2942 cm^{-1} and a week peak is observed at frequency 2946 cm^{-1} FT-IR spectrum. The symmetric CH_2 stretching vibrations are assigned to scaled vibrational frequencies at 2890 and 2874 cm^{-1} respectively. These modes are not observed experimentally both in FT-IR and FT-Raman spectrum. The scissoring vibrations are expected in the region 1455 - 1380 cm^{-1}

Table 2. Definition of local-symmetry coordinates and the values of corresponding scale factors Used to correct the B3LYP/6-311++G** (refined) force field of 2-phenyl-2-imidazoline.

No.(i)	Symbol[a]	Definition[b]	Scale factors
		Stretching	
1 - 8	ν(C-C)	R1, R2, R3, R4, R5, R6, R7, R8	0.94293
9 - 12	ν(C-N)	r9, r10, r11, r12	0.9461
13 - 17	ν(C-H)	P13, P14, P15, P16, P17	0.9225
18 - 19	ν(CH2ss)	(P18+P19)//2, (P20+P21)//2	0.9192
20 - 21	ν(CH2ass)	(P18-P19)//2, (P20-P21)//2	0.9192
22	ν(N-H)	Q22	0.91287
		In-Plane bending	
23	βR1tri	$(\beta_{23}-\beta_{24}+\beta_{25}-\beta_{26}+\beta_{27}-\beta_{28})/\sqrt{6}$	0.96557
24	βR1sym	$(-\beta_{23}-\beta_{24}+2\beta_{25}-\beta_{26}-\beta_{27}+2\beta_{28})/\sqrt{12}$	0.96557
25	βR1asy	$(\beta_{23}-\beta_{24}+\beta_{27}-\beta_{28})/2$	0.96557
26	R2bend1	$\beta_{29}+a(\beta_{30}+\beta_{33})+b(\beta_{31}-\beta_{32})$	0.956
27	R2bend2	$(a-b)(\beta_{30}-\beta_{33})+(1-a)(\beta_{31}+\beta_{32})$	0.956
28 - 33	bCH	$(\theta_{34}-\theta_{35})/\sqrt{2},(\theta_{36}-\theta_{37})/\sqrt{2},(\theta_{38}-\theta_{39})/\sqrt{2}$ $(\theta_{40}-\theta_{41})/\sqrt{2},(\theta_{42}-\theta_{43})/\sqrt{2},(\theta_{44}-\theta_{45})/\sqrt{2}$	0.9466
34	bNH	$(\theta_{46}-\theta_{47})/\sqrt{2}$.	0.9466
35 - 36	bCC	$(\theta_{48}-\theta_{49})/\sqrt{2},(\theta_{50}-\theta_{51})/\sqrt{2}$	0.9265
37 - 38	bCH2sc	$\alpha_{52}+\alpha_{53}+\alpha_{54}+\alpha_{55},\alpha_{56}+\alpha_{57}+\alpha_{58}+\alpha_{59}$	0.95715
39 - 40	bCH2Roc	$\alpha_{52}+\alpha_{53}-\alpha_{54}-\alpha_{55},\alpha_{56}+\alpha_{57}-\alpha_{58}-\alpha_{59}$	0.95715
41 - 42	bCH2Wag	$\alpha_{52}-\alpha_{53}-\alpha_{54}+\alpha_{55},\alpha_{56}-\alpha_{57}-\alpha_{58}+\alpha_{59}$	0.95715
		Out of plane bending	
43 - 47	ωC-H	ω_{60}, ω_{61}, ω_{62}, ω_{63}, ω_{64}	0.9654
48	ωN-H	ω_{65}	0.9654
49 - 50	ωC-C	ω_{66}, ω_{67}	0.98700
		Torsion	
51	τR1tri	$(\tau_{68}-\tau_{69}+\tau_{70}-\tau_{71}+\tau_{72}-\tau_{73})/\sqrt{6}$	0.98867
52	τR1asy	$(\tau_{68}-\tau_{70}+\tau_{71}-\tau_{73})/2$	0.98867
53	τR1sym	$(-\tau_{68}-2\tau_{69}-\tau_{70}-\tau_{71}+2\tau_{72}-\tau_{73})/\sqrt{12}$	0.98867
54	R2torsion1	$\tau_{76}+b(\tau_{74}+\tau_{78})+a(\tau_{75}+\tau_{77})$	0.9966
55	R2torsion2	$(a-b)(\tau_{75}-\tau_{77})+(1-a)(\tau_{74}-\tau_{78})$	0.9966
56	τCH_2	$\tau_{79}+\tau_{80}$	0.980
57	τCCCC	$\tau_{81}+\tau_{82}$	1.2000

a = cos144˚, and b = cos72˚.

and consist of medium intense bands [25] [28] [29]. In **Table 3**, CH_2 scissoring vibration has been assigned to scaled frequency at 1447 cm^{-1} and the corresponding frequency is observed at 1454 cm^{-1} in FT-Raman spectrum. The CH_2 twisting vibration and is predicted theoretically at 1004 cm^{-1} and it is observed at

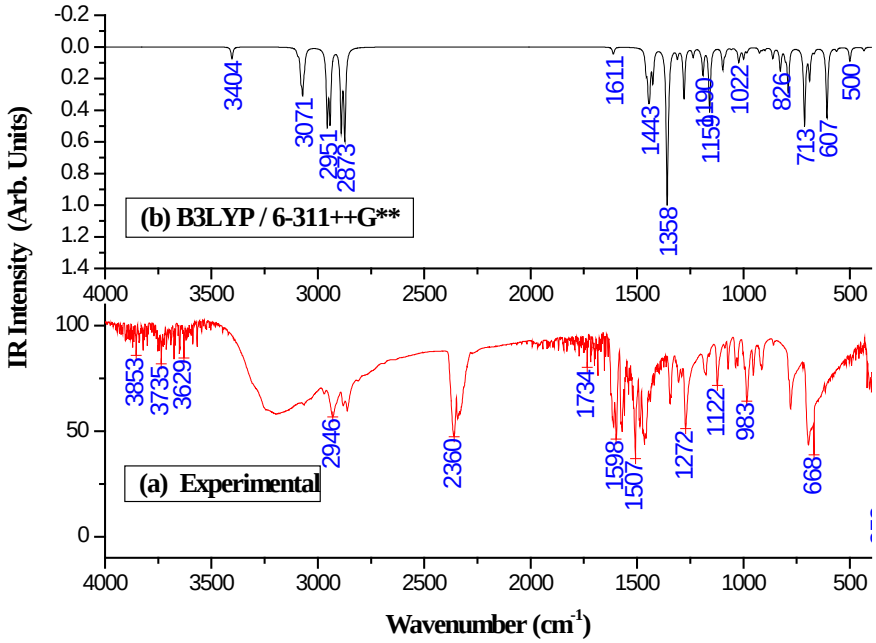

Figure 3. (a) Experimental, (b) Simulated FT-IR spectra of 2-phenyl-2-imidazoline.

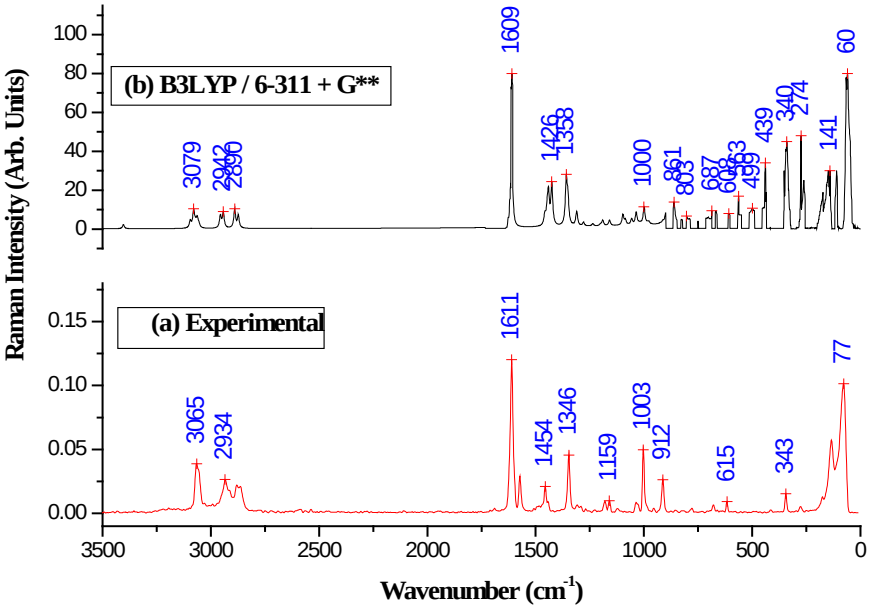

Figure 4. (a) Experimental and (b) simulated FT-Raman spectra of 2-phenyl-2-imidazoline.

1003 cm^{-1} in FT-Raman spectrum. This shows an excellent agreement with each other. The CH_2 wagging vibrations are observed theoretically with less PED distribution.

4.2.3. C-C Vibrations

The bands between 1400 and 1650 cm^{-1} in benzene derivatives are due to C-C stretching vibrations [30] [31]. The strong FT-RAMAN band at 1611 cm^{-1} and a weak FT-IR band at 1598 cm^{-1} are assigned to C-C stretching vibration and are

Table 3. Detailed assignments of fundamental vibrations of 2-phenyl-2-imidazoline by normal mode analysis based on SQM force field calculations using B3LYP/6-311++G**.

s.no	Experimental (cm^{-1})		Scaled frequencies (cm^{-1})	Intensity		Characterization of normal modes with PED (%)[a,d]
	FT-IR	FT-Raman		I_{IR}[b]	I_{RA}[c]	
1.	3404vw		3398	0.033	1.12	vNH(89)
2			3096	0.055	4.67	vCH(99)
3			3081	0.205	9.44	vCH(99)
4			3072	0.309	6.51	vCH(99)
5		3065w	3063	0.158	7.04	vCH(99)
6			3054	0.049	3.65	vCH(99)
7.			2955	0.511	7.62	vCH2as(78),vCH2ss(18)
8	2946w		2942	0.496	9.02	vCH2as(65), vCH2ss(30)
9			2890	0.546	10.4	vCH2ss(75), vCH2as(21)
10			2874	0.59	7.46	vCH2ss(59), vCH2as(26), bR2sym(10)
11			2192	0.001	0.45	gCC(61), tCCCC(38)
12	1598w	1611s	1605	0.021	20.8	vCC(69), bCH(17), bR1sym(10)
13			1582	0.003	2.02	vCC(50), vCN(15), bR2sym(14), bCH(10)
14			1473	0.029	2.43	bR2sym(25), vCC(22), bCH(20), vCN(16), gCC(10)
15		1454w	1447	0.339	16.4	bCH2sc(29), bR2sym(25), gCC(16), vCN(14), tCCCC(10)
16			1446	0.353	17.6	vCN(51), bR2sym(26), bCH2sc(15)
17			1428	0.208	20.9	vCN(39), bR2sym(20), bCH(15), vCC(12)
18			1382	0.053	2.95	bR2sym(35), vCC(16), vCN(12), gC(11)
19		1346s	1355	0.720	24.2	vCN(49), bR2sym(37)
20			1308	0.069	7.83	vCN(38), vCC(27), bR2sym(18)
21	1272s		1279	0.331	3.61	bR2sym(31), vCC(22), vCN(14), bCH2wa(10)
22			1263	0.037	1.82	bR2sym(31), vCC(22), vCN(14), bCH2wa(10)
23			1230	0.033	2.12	bNH(28)vCN(27), bR2sym(26)
24			1194	0.121	3.74	vCN(51), gCC(13), bCH2wa(10)
25		1159w	1168	0.107	2.53	vCN(49), tCH2(22), bCH2wa(12)
26			1142	0.038	2.09	bCH(66), vCC(14)
27	1122w		1122	0.016	2.13	bCH(86), vCC(11)
28			1092	0.085	5.58	bCH(28), bR2sym(21), bCH2wa(17), vCC(15)
29			1065	0.012	3.27	vCN(53), vCC(22)
30			1052	0.013	4.38	vCN(35), vCC(32), bCH(18)
31			1017	0.065	4	vCC(46), bCH(17), bR1tri(17), vCN(14)
32		1003s	1004	0.049	7.41	bCH2Ro(48), tR2asy(19), tCCCC(13)
33			997	0.067	10.1	bR1tri (49), vCC(42)
34	983s		986	0.035	4.24	gCH(68), tR1tri(21)
35			955	0.005	2.71	gCH(41), tCCCC(30)
36		912s	915	0.023	4.33	gCH(65)
37			910	0.021	4.79	vCC(60), vCN(27)

Continued

38			840	0.027	0.37	gCH(39), bR2sym(28), tCCCC(13), vCC(13)
39			839	0.0294	0.37	bR2sym(52), vCC(20), vCN(19)
40			805	0.0837	0.37	vCN(44), bR2sym(22), tR1tri(17)
41			790	0.289	5.4	vCN(67), bR2sym(10)
42			769	0.0234	1.4	vCN(44), gCC(24), bR2sym(16), tCCCC(13)
43			720	0.172	3.6	gCH(55), vCN(23)
44			694	0.135	5.29	bR2sym(49), vCN(33)
45	668w		660	0.0228	3.8	bR2sym(61), vCN(18)
46		615w	621	0.0575	4.2	bR1asy(69)
47			592	0.0459	1.65	bR2sym(42), vCN(35), gCC(13)
48			522	0.00727	4	bR2sym(44), vCN(39)
49			477	0.00617	0.52	bR2sym(55), vCN(41)
50			450	0.00435	10.8	tCCCC(94)
51		343w	347	0.0162	32	bR2sym(68), vCN(31)
52			310	0.0102	0.61	bR2sym(42), vCN(41)
53			276	0.367	35	bR2sym(34), tCCCC(28), tR2asy(18), tR2sym(12)
54			169	0.0199	11	tCCCC(67), tCH2(14), tR2asy(11)
55			142	0.0416	17	bR2sym(58), vCN(19), tCCCC(12)
56			115	0.0344	18	tCCCC(40), bR2sym(36)
57		77s	77	0.00256	4	tCCCC(100)

[a]Abbreviations: v, stretching; b, in plane bending; g, out of plane bending; t, torsion; ss, symmetrical stretching; as, asymmetrical stretching; tri, trigonal deformation; sym, symmetrical deformation; asy, asymmetric deformation, vs, very strong; s, strong; m, medium; w, weak; vw, very weak; [b]Relative absorption intensities normalized with highest peak absorption equal to 1. [c]Relative Raman intensities calculated by Equation (1) and normalized to 100. [d]Only PED contributions ≥10% are listed.

theoretically observed at frequency 1605 cm^{-1}. The remaining C-C stretching vibrations are observed theoretically at 1582 cm^{-1} and 1012 cm^{-1} and some of the frequencies are having less PED distribution. The C-C out of plane vibration predicted theoretically at 2192 cm^{-1} and no Experimental bands were observed.

4.2.4. N-H Vibrations

Hetero cyclic compound having an N-H group shows its stretching absorption in the region 3500 - 3200 cm^{-1} [32]. The peak of absorption in this region depends on the degree of hydrogen bonding along with the physical state of the sample or the Polarity of the solvent. A very weak band observed at 3404 cm^{-1} in FT-IR spectrum and the scaled frequency at 3398 cm^{-1} are assigned to N-H stretching vibrations. Further, the N-H in plane bending modes are scaled at 1230 cm^{-1}.

4.2.5. Ring Vibrations

The ring stretching vibrations have great significance during the Infrared spectrum of benzene derivatives since ring stretching vibrations include high characteristic modes of the aromatic rings. As a result of the substitution to the

aromatic ring of benzene derivatives several ring vibrations be affected. The skeletal vibrations are due to the coupled vibrations in the six ring carbon atoms. The semi circle stretching vibrations such as ring C=C and C-C vibrations take place in the region 1400 - 1625 cm^{-1}. Due to the electro negativity of nitrogen atom there are small changes in frequencies are observed for these modes. Apart from ring C-C stretching modes, trigonal deformation for related benzene ring, symmetric and asymmetric deformation modes for both the rings are assigned as listed in **Table 3**.

5. NBO Analysis

NBO analysis for the title compound was carried out at the 6-311++G** basis set to calculate delocalization of the electron density within the molecule. NBO calculations are used to understand the interactions between filled and virtual orbitals of one subsystem with another subsystem. These interactions possibly will enhance the analysis of intra- and inter molecular interactions. The hyperconjugative interaction energy is deduced from the second-order perturbation approach [33] [34]. The intramolecular hyper interactions are formed by the orbital overlap between bonding (C-C), (C-N) and (C-C), (C-N) anti bonding orbital which effects intramolecular charge transfer (ICT) causing stabilization of the system.

These interactions are observed as raise in electron density (ED) in C-C, C-N antibonding orbital to weaken the particular bonds. As listed in **Table 4**, the hyper conjugative interaction between C2-N10 and C3-C4 leads to stabilization energy of 8.65 KJ/mol. The anti bonding orbital of σ* C4-C7 and C8-C9 in conjugation with bonding orbital C5-C6 show the strong delocalization of 19.94 and 21.05 KJ/mol respectively. Similarly the anti bonding orbital of σ* C4-C7 and C5-C6 in conjugation with bonding orbital C8-C9 leads to the strong delocalization of 20.44 and 18.58 KJ/mol. respectively. Further, the σ*(C4-C7) of the NBO in conjugation with σ*(C3-N10) resulting a strong stabilization energy of 118.65 KJ/mol. These data signifies the strong hyperconjugative intramolecular interactions in the molecule and explains the stability of the molecule.

6. NLO Properties

Non linear optical (NLO) materials play a vital role in optical switching devices and industrial applications. The first hyperpolarizability β, dipole moment μ as well as polarizability α are computed using HF/6–31G (d, p) basis set on the basis of the finite-field approach. The complete equations for calculating the magnitude of total static dipole moment μ, the mean polarizability α_0, the anisotropy of the polarizability $\Delta\alpha$ and the mean first hyperpolarizability β_0, using the *x*, *y*, *z* components from Gaussian 03W output are as follows

$$\mu = \mu_x^2 + \mu_y^2 + \mu_z^2 \tag{2}$$

$$\alpha_o = \frac{\alpha_{xx} + \alpha_{yy} + \alpha_{zz}}{3} \tag{3}$$

Table 4. Second order perturbation theory analysis of fock matrix in NBO basis for 2-phenyl-2-imidazoline.

Donor(i)	Type	E_d/e	Acceptor(j)	Type	E_d/e	$E^{(2)a}$ (kJ·mol^{-1})	E(i)-E(j)^b(a.u)	f(I,j)^c(a.u)
C1-C2	σ	1.98898	N11-H12	σ^*	0.01847	2.68	1.05	0.047
C1-N11	σ	1.98586	C3-C4	σ^*	0.03966	4.34	1.18	0.064
C1-H13	σ	1.98923	C2-H21	σ^*	0.02002	1.60	0.97	0.035
C1-H20	σ	1.98675	C3-N11	σ^*	0.04973	1.59	0.95	0.035
C2-N10	σ	1.98133	C3-C4	σ^*	0.03966	8.65	1.14	0.089
C2-H14	σ	1.98369	C3-N10	σ^*	0.23563	1.74	0.55	0.029
C2-H21	σ	1.97896	C3-N10	σ^*	0.23563	2.00	0.55	0.031
C3-C4	σ	1.97168	C2-N10	σ^*	0.01298	2.98	1.03	0.050
	σ	1.97168	C3-N10	σ^*	0.01771	2.23	1.28	0.048
	σ	1.97168	C4-C5	σ^*	0.02151	2.21	1.23	0.047
	σ	1.97168	C4-C7	σ^*	0.02205	2.27	1.23	0.047
C3-N10	σ	1.98849	C3-C4	σ^*	0.03966	2.77	1.33	0.055
C3-N10	σ	1.93659	C2-H14	σ^*	0.01479	2.86	0.78	0.043
	σ	1.93659	C2-H21	σ^*	0.02002	3.53	0.77	0.047
	σ	1.93659	C4-C7	σ^*	0.37095	7.54	0.34	0.049
C4-C5	σ	1.97274	C3-C4	σ^*	0.03966	2.46	1.16	0.048
	σ	1.97274	C3-N11	σ^*	0.04973	2.55	1.12	0.048
	σ	1.97274	C4-C7	σ^*	0.02205	3.83	1.25	0.062
	σ	1.97274	C5-C6	σ^*	0.01431	2.35	1.27	0.047
C4-C7	σ	1.97515	C3-C4	σ^*	0.03966	2.28	1.17	0.046
	σ	1.97515	C3-N10	σ^*	0.01771	2.05	1.31	0.046
	σ	1.97515	C4-C5	σ^*	0.02151	3.79	1.26	0.062
	σ	1.97515	C7-C9	σ^*	0.01479	2.59	1.27	0.051
	σ	1.97515	C9-H19	σ^*	0.01209	2.16	1.17	0.045
C4-C7	σ	1.65029	C3-N10	σ^*	0.23563	16.97	0.30	0.065
	Σ	1.65029	C5-C6	σ^*	0.29661	19.17	0.29	0.067
	σ	1.65029	C8-C9	σ^*	0.32715	19.81	0.28	0.067
C5-C6	σ	1.98034	C3-C4	σ^*	0.03966	3.50	1.52	0.065
	σ	1.98034	C4-C5	σ^*	0.02151	2.82	1.27	0.053
	Σ	1.98034	C6-C8	σ^*	0.01603	2.52	1.27	0.050
	σ	1.98034	C8-H17	σ^*	0.01217	2.29	1.17	0.046
C5-C6	σ	1.65967	C4-C7	σ^*	0.37095	19.94	0.28	0.067
	σ	1.65967	C8-C9	σ^*	0.32715	21.05	0.28	0.069
C5-H15	σ	1.98061	C4-C7	σ^*	0.02205	4.31	1.08	0.061
	σ	1.98061	C6-C8	σ^*	0.01603	3.65	1.09	0.056
C6-C8	σ	1.98120	C5-C6	σ^*	0.01431	2.54	1.28	0.051
	σ	1.98120	C5-H15	σ^*	0.01359	2.31	1.19	0.047
	σ	1.98120	C8-C9	σ^*	0.01572	2.43	1.27	0.050
C6-H16	σ	1.98266	C4-C5	σ^*	0.02151	3.80	1.09	0.058

Continued

	σ	1.98266	C8-C9	σ^*	0.11572	3.54	1.10	0.056
C7-C9	σ	1.97999	C3-C4	σ^*	0.03966	3.45	1.17	0.057
	σ	1.97999	C4-C7	σ^*	0.02205	3.09	1.27	0.056
C7-H18	σ	1.98179	C4-C5	σ^*	0.02151	4.07	1.10	0.060
	σ	1.98179	C8-C9	σ^*	0.01572	3.51	1.10	0.056
C8-C9	σ	1.98101	C6-C8	σ^*	0.01603	2.42	1.27	0.049
	σ	1.98101	C7-C9	σ^*	0.01476	2.59	1.27	0.051
	σ	1.98101	C7-H18	σ^*	0.01312	2.35	1.17	0.047
C8-C9	σ	1.66151	C4-C7	σ^*	0.37095	20.44	0.28	0.068
	σ	1.66151	C5-C6	σ^*	0.29661	18.58	0.29	0.066
C8-H17	σ	1.98315	C5-C6	σ^*	0.01431	3.50	1.11	0.056
	σ	1.98315	C7-C9	σ^*	0.01476	3.60	1.10	0.056
C9-H19	σ	1.98276	C4-C7	σ^*	0.02205	3.78	1.09	0.057
	σ	1.98276	C6-C8	σ^*	0.01603	3.53	1.10	0.056
N11-H12	σ	1.98046	C3-N10	σ^*	0.01771	2.62	1.25	0.051
	σ	1.98046	C3-N10	σ^*	0.01771	2.14	0.69	0.036
LP								
N10(1)	σ	1.91978	C1-C2	σ^*	0.02495	4.86	0.70	0.053
	σ	1.91978	C3-N11	σ^*	0.04973	11.92	0.78	0.087
N11(1)	σ	1.81255	C1-H13	σ^*	0.02044	4.37	0.74	0.053
	σ	1.81255	C1-H20	σ^*	0.01525	3.21	0.75	0.046
	σ	1.81255	C3-N10	σ^*	0.23563	29.04	0.34	0.090
C4-C7	σ^*	0.37095	C3-N10	σ^*	0.23563	118.65	0.02	0.070
C5-C6	σ^*	0.29661	C5(4)	π^*	0.00043	2.09	0.87	0.099
	σ^*	0.29661	C6(4)	π^*	0.00037	2.13	0.72	0.091

[a]$E^{(2)}$ means energy of hyper conjugative interaction (stabilization energy). [b]Energy difference between donor and acceptor i and j NBO orbitals. [c]F(i, j) is the Fock matrix element between i and j NBO orbitals.

$$\Delta\alpha = 2^{-1/2}\left[\left(\alpha_{xx}-\alpha_{yy}\right)^2+\left(\alpha_{yy}-\alpha_{xx}\right)^2+6\alpha_{xx}^2\right]^{1/2} \tag{4}$$

$$\beta = \left(\beta_x^2+\beta_y^2+\beta_z^2\right)^{1/2} \tag{5}$$

and

$$\beta_x = \beta_{xxx}+\beta_{xyy}+\beta_{xzz} \tag{6}$$

$$\beta_y = \beta_{yyy}+\beta_{xxy}+\beta_{yzz} \tag{7}$$

$$\beta_z = \beta_{zzz}+\beta_{xxz}+\beta_{yyz} \tag{8}$$

The calculated first hyperpolarizability of the 2PI using HF/6-31G(d, p) is $1.0043389 \times 10^{-30}$ esu and the dipole moment is 5.70065 Debye shown in **Table 5** and **Table 6**. The calculated first hyperpolarizability of 2PI is 14 times greater than the hyperpolarizability of urea. This shows that the 2PI is useful as a non

Table 5. The calculated quantum chemical parameters for 2-phenyl-2-imidazoline obtained by B3LYP/6-311++G** calculations.

Property	2-phenyl-2-imidazoline
Total energy (eV)	−12401.75816
E_{HOMO} (eV)	−5.82160670
E_{LUMO} (eV)	−0.78749789
E_{HOMO}-E_{LUMO} (eV)	5.03410881
Electronagativity (χ) eV	3.304552295
Chemical hardness (η) eV	−2.517054405
Electrofilicity index (ω) eV	−2.1692153035
Global Softness (σ)eV	−0.3972897836
Total energy change (ΔE_T) eV	0.62926360125
Dipole moment (D)	5.70065

Table 6. The electric dipole moment μ(D) the average polarizability α_{tot} ($\times 10^{-12}$ esu) and the first hyperpolarizability β_{tot} ($\times 10^{-30}$ esu) of 2-phenyl-2-imidazoline by HF/6-311++G** method.

μ and α components	HF/6-31G(d,p)	β components	HF/6-31G(d,p)
μ_x	0.104085	β_{xxx}	−91.4409918
μ_y	0.2171718	β_{xxy}	−14.7087352
μ_z	−1.065635	β_{xyy}	−44.654681
$\mu(D)$	1.19357523	β_{yyy}	0.6127935
α_{xx}	143.1369019	β_{xxz}	−65.4861453
α_{xy}	4.2163498	β_{xyz}	17.3286849
α_{yy}	56.0399983	β_{yyz}	−2.0474112
α_{xz}	−6.356907	β_{xzz}	56.4680477
α_{yz}	17.5520362	β_{yzz}	11.6736082
α_{zz}	96.5295611	β_{zzz}	−17.1315722
α(esu)	$14.607899 \times 10^{-12}$ esu	β total (esu)	$1.0043389 \times 10^{-30}$ esu

linear optical material.

7. Electronic Absorption Spectra

Both the highest occupied molecular orbital (HOMO) and lowest unoccupied molecular orbital (LUMO) are the main orbitals take part in chemical stability [35]. The chemical activity of the molecule is revealed from the HOMO-LUMO energy gap. The HOMO stands for the ability to donate an electron and the LUMO stands for the ability to accept an electron. The HOMO-LUMO energy gap and other molecular properties of 2PI calculated at the DFT/B3LYP method with 6-311++G** level is shown in Table 5. The atomic orbital components of the frontier molecular orbital (HOMO—MO: 39, LUMO—MO: 40) and the Visualization of the molecular orbitals [MO: 32–MO: 47] of 2-phenyl-2-imidazoline under C_1 symmetry are shown in Figure 5 and Figure 6 respectively.

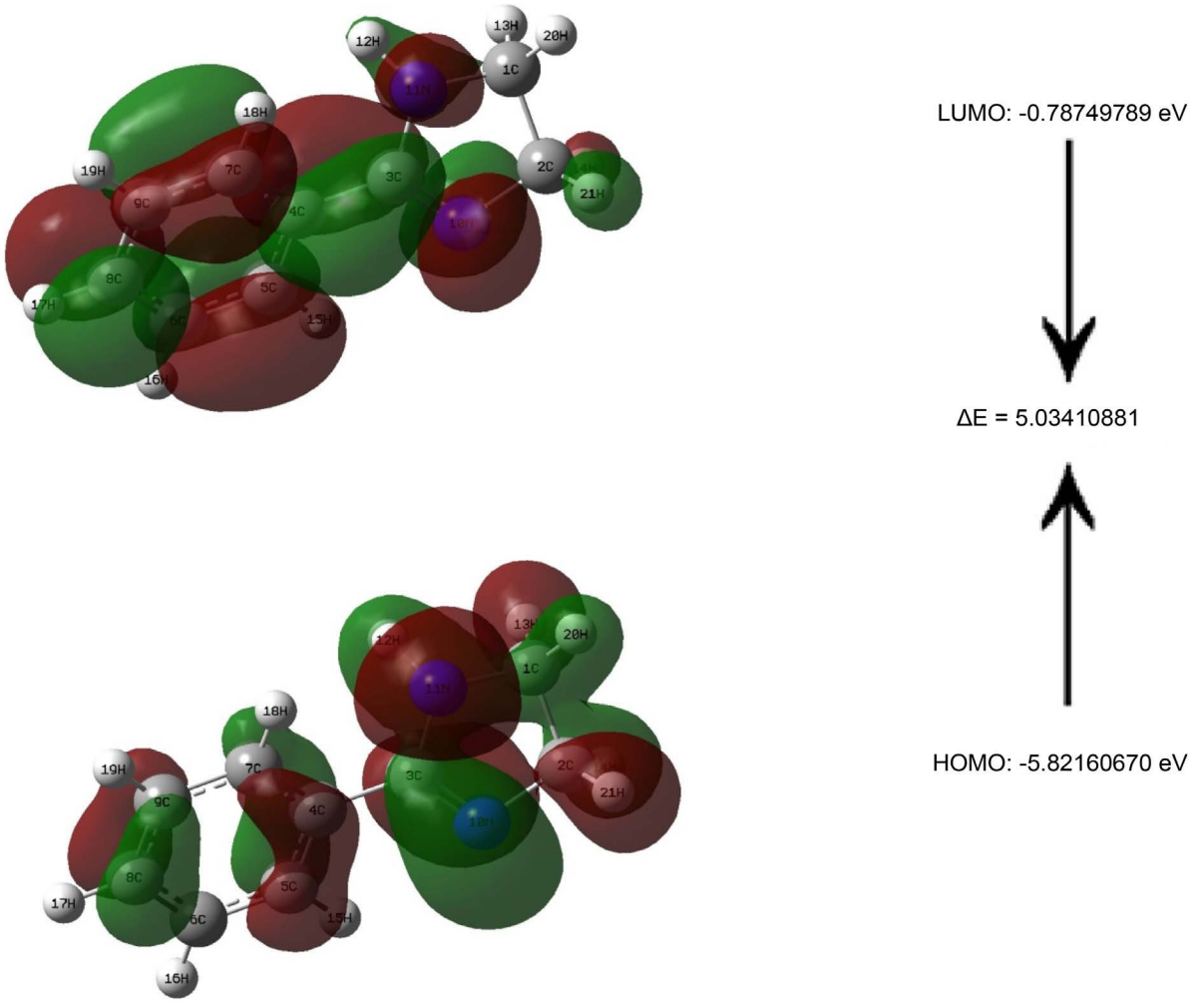

Figure 5. The atomic orbital components of the frontier molecular orbital (HOMO—MO: 39, LUMO—MO: 40) of 2-phenyl -2-imidazoline.

The UV-Visible absorption spectrum of the title molecule using SAC CI/6-311++G** basis set is performed to determine the lower lying excited states. The computed results involving the vertical excitation energies, oscillator strength (f) and wavelength are carried out and compared with measured investigational wavelength. These are presented in **Table 7**. In accordance with Frank-Condon Principle, the maximum absorption peak correspond in UV-vis spectrum to vertical excitation were carried out SAC-CI method and calculated one strong electronic transition at 272.60 nm with an oscillator strength f = 0.0658, shows good agreement with measured experimental data (exp = 273 nm) as shown in **Figure 7**. The addition of strong electron-withdrawing C-N substituent at the 2-position not only leads to a large red shift in Imidazoline UV-Vis absorption spectra but it also increases the light absorption efficiency of compound, owing to the facilitation of intramolecular charge transfer (ICT).

Molecular electrostatic potential (MEP) mapping is very useful in the investigation of the molecular structure with its physiochemical property relationships

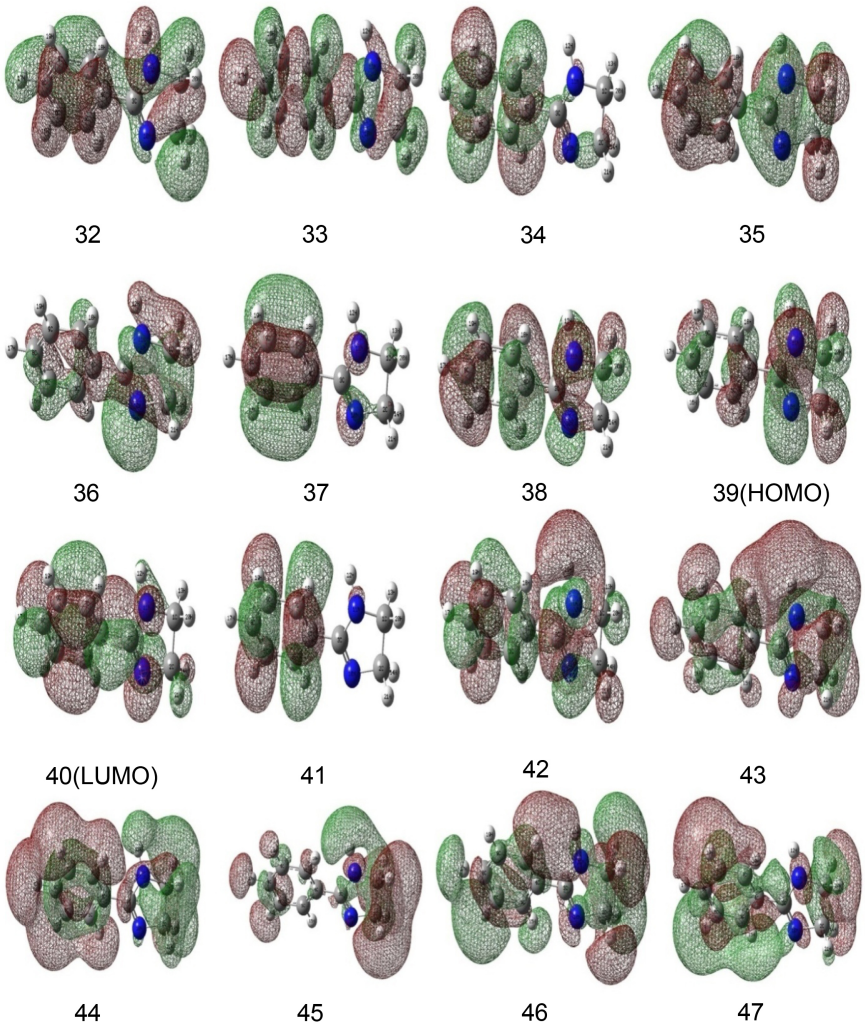

Figure 6. Visualization of the molecular orbitals [MO: 32-MO: 47] of 2-phenyl-2-imidazoline under C_1 symmetry: HOMO-MO: 39 and LUMO-MO: 40.

[36]-[41]. The significance of MEPs is that it concurrently shows molecular shape, size in addition to positive, negative and neutral electrostatic potential areas. The Molecular electrostatic potential (MEP) mapping of the title compound was shown in **Figure 8**. MEP is very useful in research of molecular structure with its physicochemical property relationship [42] [43]. The molecular electrostatic potential $V(r)$ at a position r because of a molecular structure having charges of the nuclei $\{Z_A\}$ positioned at point $\{R_A\}$ and the electron density $\rho(r)$ is specified by

$$V(r)=\sum_A^N\left[\left(Z_A/|r-R_A|-\int\rho(r')\mathrm{d}^3r'/|r-r'|\right)\right] \tag{9}$$

8. Thermodynamic Properties

On the basis of vibrational analyses and statistical thermodynamics, the standard thermodynamic functions: heat capacity, internal energy, entropy and enthalpy were calculated using Moltranv. 2.5 [44] and are listed in **Table 8**. It is observed

Table 7. The UV-vis excitation energy and oscillator strength for 2-phenyl-2-imidazalone calculated by SAC CI method.

No.	Exp. Wavelength	Energy (cm^{-1})	Wavelength (nm)	Osc. Strength	Symmetry	Major contrib.
1	273.00	36,683.15536	272.60	0.0658	Singlet-A	HOMO- > LUMO (92%) H-1- > LUMO (5%)
2	--	41,541.06624	240.72	0.0214	Singlet-A	H-3- > LUMO (86%) H-1- > LUMO (7%), HOMO- > LUMO (−3%)
3	--	49,875.25072	200.50	0.0059	Singlet-A	H-3- > L + 1 (90%) H-2- > L + 1 (−3%), H-1- > L + 1 (6%)
4	--	58,519.15424	170.88	0.0015	Singlet-A	H-5- > LUMO (97%)
5	--	62,270.4648	160.58	0.0074	Singlet-A	HOMO- > L + 4 (83%)H-4- > LUMO (−3%), H-3- > L + 2 (−2%), H-1- > L + 3 (−3%), HOMO- > L + 5 (−2%)
6	--	65,521.70816	152.62	0.0089	Singlet-A	HOMO- > L + 5 (72%)H-4- > LUMO (3%), H-2- > L + 3 (−3%), H-1- > L + 2 (8%), HOMO- > L + 4 (2%)
7	--	67,402.60608	148.36	0.0352	Singlet-A	H-3- > L + 3 (81%)H-1- > L + 4 (−5%)
8	--	68,145.44784	146.74	0.0067	Singlet-A	H-7- > LUMO (82%)H-9- > LUMO (6%), HOMO- > L + 6 (−2%)
9	--	69,112.51328	144.69	0.0245	Singlet-A	H-1- > L + 4 (60%), HOMO- > L + 6 (13%)H-8- > LUMO (2%), H-3- > L + 3 (3%), H-1- > L + 3 (−7%)

Table 8. Thermo dynamical properties of 2-phenyl-2-imidazoline obtained by 6-311++G** density functional calculations.

Temperature (K)	C_V (J/K/mol)	C_P (J/K/mol)	U (J/K/mol)	H (J/K/mol)	S (J/K/mol)	G (J/K/mol)
50	41.711	50.025	463.417	463.833	257.095	450.978
100	58.629	66.944	465.937	466.768	297.116	437.057
150	74.786	83.100	469.266	470.513	327.267	421.423
200	94.048	102.363	473.468	475.131	353.712	404.388
250	117.122	125.436	478.732	480.811	378.975	386.067
300	142.556	150.871	485.223	487.717	404.079	366.493
350	168.474	176.789	492.989	495.899	429.273	345.654
400	193.457	201.772	502.040	505.366	454.524	323.557
450	216.713	225.028	512.313	516.055	479.662	300.207
500	237.953	246.268	523.690	527.848	504.490	275.603

that the values of C_P, C_V, U, H and S increase with increase of temperature from 100 to 500 K. The thermo dynamical parameters were fitted with the temperature by quadratic, linear and quadratic formulas respectively.

Further thermo dynamical data provides the needful information about the molecule. Thermo dynamical data used to estimate directions of chemical reactions according second law of thermodynamics in the thermo chemical field.

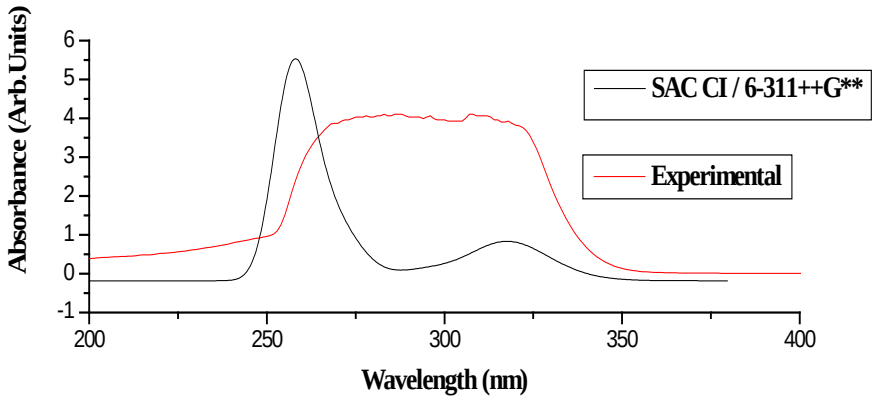

Figure 7. Theoretical and experimental UV/Vis spectra of 2-phenyl-2-imidazoline.

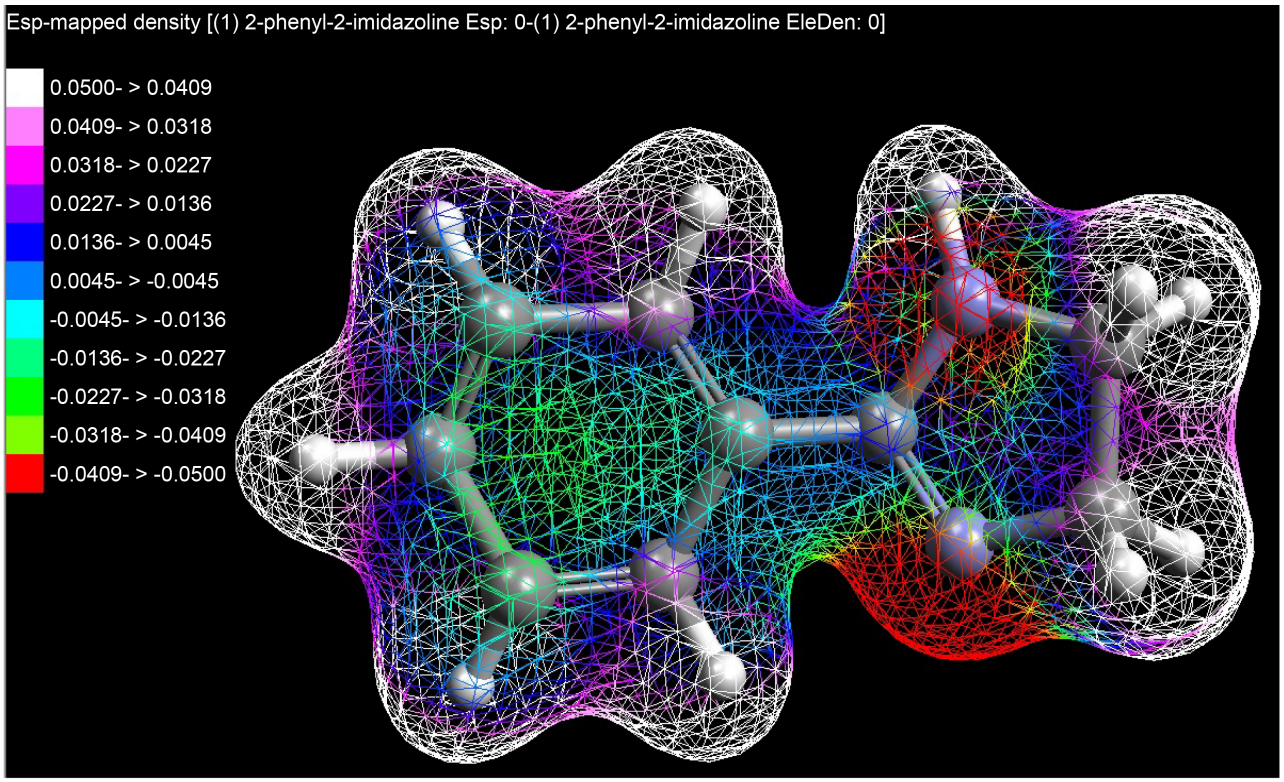

Figure 8. B3LYP/6-311++G** calculated 3D molecular electrostatic potential maps of 2-phenyl-2-imidazoline.

9. Conclusions

The theoretical and experimental FT-IR, FT-Raman spectral studies and NBO analysis of 2PI were carried out and reported. Complete vibrational analysis of 2PI was performed on the basis of DFT calculations at the B3LYP/6-311++G** level of theory and presented. The 42 normal modes of vibrations were ambiguously assigned based on the result of PED output obtained from normal coordinate analysis. There was a qualitative agreement among the calculated and observed frequencies. The NBO analysis shows strong intermolecular hyperconjugative interactions of electron. The strong delocalization of electrons in the molecule is primary to a stabilization of the molecule.

Acknowledgements

The First author, Y. Sushma Priya is thankful to Sophisticated Analytical Instrumentation Facility (SAIF), IIT Madras, Chennai and Analytical Chemistry laboratories for their services. The corresponding author, A. Veeraiah is highly grateful to Science and Engineering Research Board, Department of Science and Technology, Government of India for the financial assistance provided. Further, the authors are highly grateful to Prof. T. Sundius for Molvib program.

References

[1] Vizi, E.S. (1986) *Medicinal Research Reviews*, **6**, 431-449. https://doi.org/10.1002/med.2610060403

[2] Le Bihan, G., Rondu, F., Pele-Tounian, A., Wang, X., Lidy, S., Touboul, E., Lamouri, A., Dive, G., Huet, J., Pfeiffer, B., Renard, P., Guardiola-Lemaitre, B., Manechez, D., Penicaud, L., Ktorza, A. and Godfroid, J.-J. (1999) *Journal of Medicinal Chemistry*, **42**, 1587-1603. https://doi.org/10.1021/jm981099b

[3] Li, H.Y., Drummond, S., De Lucca, I. and Boswell, G.A. (1996) *Tetrahedron*, **52**, 11153-11162. https://doi.org/10.1016/0040-4020(96)00578-9

[4] Ueno, M., Imaizumi, K., Sugita, T., Takata, I. and Takeshita, M. (1995) *International Journal of Immunopharmacology*, **17**, 597-603. https://doi.org/10.1016/0192-0561(95)00057-9

[5] Schorderet, M. (1992) Pharmacologie: Des Concepts Fondamentaux aux Applications the Rapeutiques. Frison-Roche, Paris, 130-153.

[6] Rodríguez-Valdez, L.M., Villamisar, W., Casales, M., González-Rodriguez, J.G., Martínez-Villafañe, A., Martinez, L. and Glossman-mitnik, D. (2006) *Corrosion Science*, **48**, 4053-4064. https://doi.org/10.1016/j.corsci.2006.05.036

[7] González-Rodríguez, C.A., Rodríguez-Gómez, F.J. and Genescá-Llongueras, J. (2008) *Electrochimica Acta*, **54**, 86-90. https://doi.org/10.1016/j.electacta.2008.02.119

[8] Contreras, C.D., Montejo, M., Lopez Gonzalez, J.J., Zinczuk, J. and Brandan, S.A. (2011) *Journal of Raman Spectroscopy*, **42**, 108-116.

[9] Frisch, M.J., Trucks, G.W., Schlegel, H.B., Scuseria, G.E., Robb, M.A., Cheeseman, J.R., Scalmani, G., Barone, V., Mennucci, B., Petersson, G.A., Nakatsuji, H., Caricato, M., Li, X., Hratchian, H.P., Izmaylov, A.F., Bloino, J., Zheng, G., Sonnenberg, J.L., Hada, M., Ehara, M., Toyota, K., Fukuda, R., Hasegawa, J., Ishida, M., Nakajima, T., Honda, Y., Kitao, O., Nakai, H., Vreven, T., Montgomery, J.A., Peralta, J.E., Ogliaro, F., Bearpark, M., Heyd, J.J., Brothers, E., Kudin, K.N., Staroverov, V.N., Kobayashi, R., Normand, J., Raghavachari, K., Rendell, A., Burant, J.C., Iyengar, S.S., Tomasi, J., Cossi, M., Rega, N., Millam, J.M., Klene, M., Knox, J.E., Cross, J.B., Bakken, V., Adamo, C., Jaramillo, J., Gomperts, R., Stratmann, R.E., Yazyev, O., Austin, A.J., Cammi, R., Pomelli, C., Ochterski, J.W., Martin, R.L., Morokuma, K., Zakrzewski, V.G., Voth, G.A., Salvador, P., Dannenberg, J.J., Dapprich, S., Daniels, A.D., Farkas, Ö., Foresman, J.B., Ortiz, J.V., Cioslowski, J. and Fox, D.J. (2009) Gaussian. Wallingford.

[10] Dennington, R., Keith, T. and Millam, J. (2009) Gauss View. Version 5, Semichem Inc., Shawnee Mission.

[11] Rauhut, G. and Pulay, P. (1995) *The Journal of Physical Chemistry*, **99**, 3093-3100. https://doi.org/10.1021/j100010a019

[12] Pulay, P., *et al*. (1983) *Journal of the American Chemical Society*, **105**, 7037-7047. https://doi.org/10.1021/ja00362a005

[13] Fogarasi, G., Pulay, P. and Durig, J.R. (1985) Chapter 3, Vibrational Spectra and Structure. Elsevier, Amsterdam, Vol. 14, 125.

[14] Sundius, T. (1990) *Journal of Molecular Structure*, **218**, 321-326. https://doi.org/10.1016/0022-2860(90)80287-T

[15] Sundius, T. (2002) *Vibrational Spectroscopy*, **29**, 89-95. https://doi.org/10.1016/S0924-2031(01)00189-8

[16] Glendering, E.D., Reed, A.E., Carpenter, J.E. and Weinhold, F. (1998) NBO Version 3.1. TCI, University of Wisconsin, Madison.

[17] Polavarapu, P.L. (1990) *The Journal of Physical Chemistry*, **94**, 8106-8112. https://doi.org/10.1021/j100384a024

[18] Keresztury, G., Holly, S., Varga, J., Besenyei, G., Wang, A.Y. and Durig, J.R. (1993) *Spectrochimica Acta Part A*, **49**, 2007-2017. https://doi.org/10.1016/S0584-8539(09)91012-1

[19] Becke, A.D. (1993) *The Journal of Chemical Physics*, **98**, 5648-5652. https://doi.org/10.1063/1.464913

[20] Jing, L.-L., Ma, H.-P., He, L., Fan, P.-C. and Jia, Z.-P. (2011) *Acta Crystallographica Section E*, **67**, o3503.

[21] Pulay, P., Fogarasi, G., Pang, F. and Boggs, J.E. (1979) *Journal of the American Chemical Society*, **101**, 2550.

[22] Fogarasi, G., Zhou, X., Taylor, P.W. and Pulay, P. (1992) *Journal of the American Chemical Society*, **114**, 8191-8201. https://doi.org/10.1021/ja00047a032

[23] Lambert, J.B., Shurvell, H.F., Verbit, L., Cooks, R.G. and Stout, G.H. (1976) Organic Structural Analysis. Macmillan Publ. Co. Inc., New York.

[24] Silverstein, R.M., Basseler, G.C. and Morill, C. (1981) Spectrometric Identification of Organic Compounds. John Wiley and Sons, New York.

[25] Veeraiah, A. (2015) *Spectrochimica Acta Part A*: *Molecular and Biomolecular Spectroscopy*, **147**, 212-224. https://doi.org/10.1016/j.saa.2015.03.053

[26] Chandra, S., Saleem, H., Sebastian, S. and Sundaraganesan, N. (2011) *Spectrochimica Acta Part A*, **78**, 1515-1524. https://doi.org/10.1016/j.saa.2011.01.043

[27] Furic, K., Mohack, V., Bonifacic, M. and Stefanic, I. (1992) *Journal of Molecular Structure*, **267**, 39-44. https://doi.org/10.1016/0022-2860(92)87006-H

[28] Colthup, N.B., Daly, L.H. and Wiberley, S.E. (1990) Introduction to Infrared and Raman Spectroscopy. Academic Press, New York.

[29] Smith, B.C. (1998) Infrared Spectral Interpretation: A Systematic Approach. CRC Press, Boca Raton, FL.

[30] Socrates, G. (2001) Infrared and Raman Characteristic Group Frequencies—Tables and Charts. 3rd Edition, Wiley & Sons, Chichester.

[31] Nagabalasubramanian, P.B., Periandy, S., Mohan, S. and Govindarajan, M. (2009) *Spectrochimica Acta Part A*, **73**, 277-280. https://doi.org/10.1016/j.saa.2009.02.044

[32] Silverstein, M., Clayton Bassler, G. and Morril, C. (1981) Spectroscopic Identification of Organic Compounds. John Wiley, New York.

[33] James, C., AmalRaj, A., Reghunathan, R., Hubert Joe, I. and JayaKumar, V.S. (2006) *Journal of Raman Spectroscopy*, **37**, 1381-1392. https://doi.org/10.1002/jrs.1554

[34] Na, L.J., Rang, C.Z. and Fang, Y.S. (2005) *Journal of Zhejiang University Science B*,

6, 584-589.

[35] Gunasekaran, S., Balaji, R.A., Kumaresan, S., Anand, G. and Srinivasan, S. (2008) *Canadian Journal of Analytical Sciences and Spectroscopy*, **53**, 149-162.

[36] Murray, J.S. and Sen, K. (1996) Molecular Electrostatic Potentials, Concepts and Applications. Elsevier, Amsterdam.

[37] Alkorta, I. and Perez, J.J. (1996) *International Journal of Quantum Chemistry*, **57**, 123-135. https://doi.org/10.1002/(SICI)1097-461X(1996)57:1<123::AID-QUA14>3.0.CO;2-9

[38] Lowdin, P. (1978) Advances in Quantum Chemistry. Academic Press, New York.

[39] Luque, F.J., Orozco, M., Bhadane, P.K. and Gadre, S.R. (1993) *The Journal of Physical Chemistry*, **97**, 9380-9384. https://doi.org/10.1021/j100139a021

[40] Sponer, J. and Hobza, P. (1996) *International Journal of Quantum Chemistry*, **57**, 959-970. https://doi.org/10.1002/(SICI)1097-461X(1996)57:5<959::AID-QUA16>3.0.CO;2-S

[41] Anbarasana, P.M., Subramanian, M.K., Senthilkumar, P., Mohanasundaram, C., Ilangovan, V. and Sundaraganesan, N. (2011) *Journal of Chemical and Pharmaceutical Research*, **3**, 597-612.

[42] Murray, J.S. and Sen, K. (1996) Molecular Electrostatic Potentials, Concepts and Applications. Elsevier, Amsterdam.

[43] Scrocco, E. and Tomasi, J. (1978) Electronic Molecular Structure, Reactivity and Intermolecular Forces: An Heuristic Interpretation by Means of Electrostatic Molecular Potentials. In: Lowdin, P.O., Ed., *Advances in Quantum Chemistry*, Academic Press, New York, p. 115.

[44] Ignatov, S.K. (2004) Program for Molecular Visualization and Thermodynamic Calculations. University of Nizhny Novgorod, Nizhnij Novgorod. http://ichem.unn.ru/Moltran

Supplementary Material 1

Table S1. Definition of internal coordinates of 2-phenyl-2-imidazoline.

No.(i)	Symbol	Type	Definition[a]
			Stretching
1 - 8	R_i	CC	C1-C2, C3-C4, C4-C5, C5-C6, C6-C8, C8-C9, C4-C7, C7-C9
9 - 12	r_i	CN	C1-N11, C2-N10, C3-N11, C3-N10
13 - 21	P_i	CH	C5-H15, C6-H16, C8-H17, C9-H19, C7-H18, C1-H20, C1-H13, C2-H14, C2-H21.
22	Q_i	NH	N11-H12.
			In-Plane bending
23 - 28	β_1	Ring1	C4-C5-C6, C5-C6-C8, C6-C8-C9, C8-C9-C7, C9-C7-C4, C7-C4-C5.
29 - 33	β_1	Ring2	C1-C2-N10, C2-N10-C3, N10-C3-N11, C3-N11-C1, N11-C1-C2.
34 - 43	β_1	CCH	C4-C7-H18, C9-C7-H18, C7-C9-H19, C8-C9-H19, C9-C8-H17, C6-C8-H17, C8-C6-H16, C5-C6-H16, C4-C5-H15, C6-C5-H115, C1-C2-H14, N10-C2-H14.
44 - 47	θ_i	CN	C1-N11-H12, C3-N11-H12, N11-C3-C4, N10-C3-C4.
48 - 49	θ_i	CC	C7-C4-C3, C5-C4-C3.
50 - 53	θ_i	NCH	N11-C1-H13, N11-C1-H20, N10-C2-H14, N10-C2-H21.
54 - 55	θ_i	HCH	H13-C1-H20, H14-C2-H21.
			Out-of-plane bending
56 - 60	$\dot{\omega}_i$	CH	H15-C5-C4-C6, H16-C6-C5-C8, H17-C8-C6-C9, H19-C9-C8-C7, H18-C7-C9-C4.
61	φ_i	NH	H12-N11-C3-C1
62	π_i	CN	C4-C3-N10-N11
63	π_i	CC	C3-C4-C7-C5
			Torsion
64 - 69	τ_i	τRING1	C4-C5-C6-C8, C5-C6-C8-C9, C6-C8-C9-C7, C8-C9-C7-C4, C9-C7-C4-C5, C7-C4-C5-C6
70 - 74	τ_i	τRING2	C1-C2 -N10-C3, C2-N10-C3-N11, N10-C3-N11-C1, C3-N11-C1-C2, N11-C1-C2-N10
75 - 82	τ_i	τCH_2	C3-N11-C1-H13, C3-N11-C1-H20, N10-C2-C1-H13, N10-C2-C1-H20, N11-C1-C2-H14, N11-C1-C2-H21, C3-N10-C2-H14, C3-N10-C2-H21.
83 - 84	τ_i	Butterfly	N10-C3-C4-C7, C5-C4-C3-N11.

[a]For numbering of atom refer **Figure 1**.